11th World Congress on Computational Mechanics (WCCM XI)
5th European Conference on Computational Mechanics (ECCM V)
6th European Conference on Computational Fluid Dynamics (ECFD VI)
E. Oñate, J. Oliver and A. Huerta (Eds)

NUMERICAL MODELLING OF LAMINAR FLOW CONTROL ON A SWEPT WING BY MEANS OF PLASMA ACTUATORS

SERGEY L. CHERNYSHEV*, ALEKSANDR P. KURYACHII*, SERGEY V. MANUILOVICH*, DMITRY A. RUSYANOV*, MARAT D. GAMIRULLIN*

* Central Aerohydrodynamic Institute (TsAGI)
1, Zhukovsky str., Zhukovsky, 140180 Moscow region, Russia
e-mail: aleksandr.kuryachiy@tsagi.ru, www.tsagi.ru

Key Words: *force and heat impact, cross-flow instability.*

Abstract. Theoretical assessment of the volumetric force and heat impact of plasma actuators necessary for laminar flow control on an infinite span swept wing is presented. Calculations are carried out for geometric and free stream parameters corresponding to typical cruise flight conditions of subsonic civil airplane. The impact of plasma actuators on 3D compressible boundary layer is simulated by force and heat source terms in momentum and energy equations. The linear stability of the boundary layer flow with respect to stationary modes of the cross-flow-type disturbances is considered. The position of the laminar-turbulent transition caused by the cross-flow instability is estimated with the aid of e^N-method.

1 INTRODUCTION

A development of innovative aerodynamic technologies aimed on substantial reduction in fuel consumption and atmospheric pollution remains in the centre of attention of the aeronautical community, industry and research centers [1]. Cruise drag reduction promotes achievement this goal. The viscous drag contributes about a half of the total cruise drag of modern civil airplanes. A delaying laminar to turbulent boundary layer transition on aerodynamic surfaces is one of the effective methods of viscous drag reduction. The cross-flow-type instability is, as a rule, the main reason of laminar-turbulent transition on a swept wing [2]. Therefore any method of suppression of this instability would be a key to solution the problem of a swept wing drag reduction, if this method is energy acceptable.

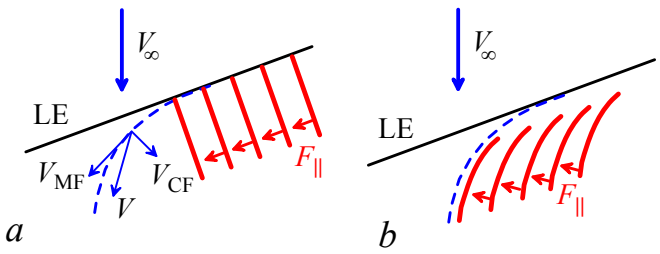

Figure 1: The concept of EGD LFC on a swept wing

The concept of laminar flow control (LFC) method proposed at TsAGI [3] and based on an attenuation of the cross-flow-type instability due to electrogasdynamic (EGD) force impact on three-dimensional boundary layer in the vicinity of a swept wing leading edge is illustrated in Fig. 1. Here $\boldsymbol{V}_\infty$ is the free-stream velocity vector, LE denotes the swept wing leading edge, $\boldsymbol{V}$ is the gas velocity vector at some point inside a boundary layer, $\boldsymbol{V}_{\mathrm{MF}}$ and $\boldsymbol{V}_{\mathrm{CF}}$ are the main-flow and cross-flow components of the velocity vector, dashed blue curve shows the external inviscid streamline.

The necessary force impact on boundary layer flow can be realized with the help of plasma actuators operating on the base of near surface dielectric barrier discharge (DBD) [4-6]. Red solid curves in Fig. 1 show the exposed electrodes of DBD-actuators, $\boldsymbol{F}_{\|}$ is the vector component of the volumetric force generated by every actuator and directed parallel to a wing surface.

The simplest arrangement of DBD actuators is shown in Fig. 1, *a*. Actuators are placed continuously both on lower and upper wing surfaces perpendicular to leading edge. Volumetric force impact directed along the leading edge will be partially opposite to cross-flow velocity $\boldsymbol{V}_{\mathrm{CF}}$. The configuration shown in Fig. 1, *b* is more geometrically complex but seems to be more effective and less energy consuming. The curvilinear actuators placed along the external streamline will generate the volumetric force $\boldsymbol{F}_{\|}$ directly against $\boldsymbol{V}_{\mathrm{CF}}$. In this case the DBD-actuators are placed beginning from the line of the cross-flow-type instability origin. In both cases an attenuation of the cross-flow velocity $\boldsymbol{V}_{\mathrm{CF}}$ results in a decrease in increments of spatial growth of the cross-flow-type instability [7]. If this decrease is significant, the laminar-turbulent transition caused by the cross-flow-type instability can be delayed or wholly removed.

Development and optimization of DBD-actuators in series creating necessary force impact over significant part of a surface along a whole wing leading edge is a substantial problem for practical realization of EGD LFC method. Experimental optimization of multi-actuator system is more complex as compared to a single actuator because of presence additional geometric and physical parameters governing a system operation [8]. The optimal design of DBD-actuators in series must ensure a discharge ignition only at one side of every exposed electrode and exclude it at the other side. To diminish damaging mutual interaction between the adjacent actuators [9] some advanced designs of multi-actuator system have been proposed [10, 11]. Experiments confirmed the effectiveness of the design with additional buried screening electrodes electrically linked with the exposed ones [10] or with additional exposed electrodes under floating potential [11].

Two essential things must be taken into consideration in development of multiple DBD actuators intended for considered LFC method. First of all, the boundary layer thickness in the vicinity of a wing leading edge both on real airplane at cruise flight conditions and on a wing models in wind tunnel tests is very small (less than 1 mm). Therefore the main sizes of multi-actuator system such as the width of the exposed electrodes and the distance between them must be small enough in order to ensure a concentration of the volumetric force generated in DBD wholly inside a boundary layer. Furthermore, DBD actuators are supposed to be placed over a wing skin which must be electroconductive because of airplane electrostatic safety requirements.

Simple design of multi-actuator system proposed in [12] uses the mentioned above concept of additional screening buried electrodes but unlike [10] takes into account theirs assumed

application on airplane wing and seems to be more effective. The scheme of the proposed multi-actuator system is shown in the left Fig. 2 and consists of the continuous accelerating electrode common for all actuators in series (lower blue layer), the narrow exposed electrodes (upper red rectangles), the narrow buried screening electrodes (inner red rectangles), two dielectric layers, and the glue layer between dielectrics. The metallic or composite electroconductive wing skin being under constant (zero) electric potential can serve as common accelerating electrode. The alternating electric potential is applied to the exposed and screening electrodes. The last prevent the discharge ignition near the left edges of the exposed electrodes. Therefore the average horizontal force $F_{\parallel}$ generated by actuators accelerates the gas flow from left to right over a whole surface.

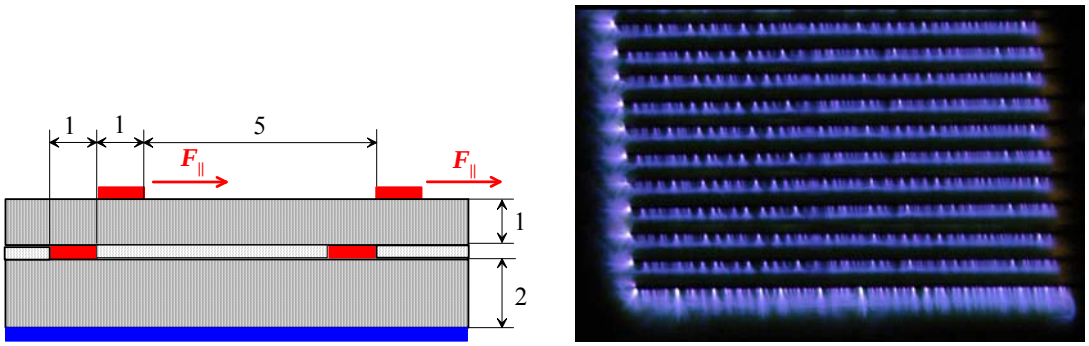

Figure 2: The scheme of multi-actuator system (left) and the picture of DBD on 11 actuators (right)

The right Figure 2 demonstrates an operability of the proposed scheme containing 11 actuators with the sizes in millimeters shown in the left picture. The amplitude and the frequency of the alternating voltage applied to the exposed and screening electrodes equal 8 kV and 10 kHz, respectively. It is seeing that the discharge fluorescence is observed only near one edge (bottom in the picture) of every exposed electrode. The presented experimental results permit to use main geometric parameters of multi-actuator system close to sizes indicated above in the subsequent numerical modeling.

Experimental research and optimization of the considered LFC method both in wind tunnels and flight tests is very expensive because of numerous geometrical and physical parameters governing this method. Therefore numerical simulation seems to be relevant for preliminary estimations of this method effectiveness. In the strict sense numerical modeling of the dielectric barrier discharge actuators is necessary in order to calculate spatial distributions of volumetric force and energy release with subsequent their use in boundary layer calculations [13]. But such modeling even for one set of geometrical and physical parameters of DBD-actuator is very time consuming [14]. Therefore analytical approximations for volumetric force and heat release predicted by phenomenological models of DBD are used, as a rule, in modeling of DBD impact on air flows [15]. This approach seems to be reasonable in preliminary parametric study of EGD LFC method and is used in the present work.

2 BOUNDARY LAYER CALCULATIONS

The effect of DBD-actuators on cross-flow-type instability and laminar-turbulent transition is estimated by the example of flow over an infinite span swept wing with the sweep angle

$\chi = 30^o$. The static pressure $p_\infty = 2.6 \cdot 10^4$ Pa, the air temperature $T_\infty = 223$ K corresponding to flight altitude about 10 km, and Mach number $M_\infty = 0.8$ are taken as the main free-stream parameters. They determine other flow parameters necessary for further boundary layer calculations: the flow velocity $V_\infty = 240$ m/s, the air density $\rho_\infty = 0.41$ kg/m^3, the dynamic viscosity coefficient $\mu_\infty = 1.33 \cdot 10^{-5}$ kg/(m·s).

The external boundary conditions for calculations of the compressible boundary layer have been obtained from the calculation of 2D inviscid flow over LV6 DLR airfoil at zero angle of attack on the base of the Euler equations. It is supposed that volumetric and force impact of plasma actuators is concentrated entirely inside a boundary layer. The spanwise modulation of the boundary layer displacement thickness resulting from actuators impact and corresponding viscous-inviscid interaction is not taken into consideration.

The boundary layer flow in the vicinity of a wing leading edge is characterized by Reynolds number $\mathrm{Re} = \rho_\infty V_\infty l/\mu_\infty$ determined by streamwise length $l = V_\infty/[du_e(0)/dx]$ (equals approximately a half radius of the leading edge curvature), where the x-coordinate is directed along a wing surface perpendicular to a leading edge, and u_e is the x-component of the external velocity obtained from inviscid calculation. The airfoil chord length normal to a leading edge L is related with the characteristic length l as $L = l\, du_e^{/}(0)/dx^{/}$, where the dimensionless velocity $u_e^{/}$ and the coordinate $x^{/}$ are measured in $V_\infty \cos\chi$ and L, respectively. According to executed 2D inviscid flow calculation, $du_e^{/}(0)/dx^{/} = 107.7$. The value $l = 0.03$ m is taken in the present estimations, hence, the airfoil chord length equals $L = 3.23$ m.

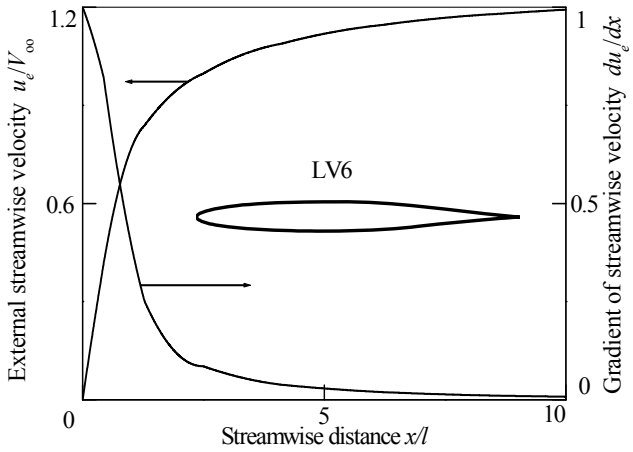

Figure 3: Dimensionless external streamwise velocity and its streamwise gradient

Calculated distributions of the non-dimensional x-component of the external flow velocity $u_e^* = u_e/V_\infty$ in the vicinity of the wing leading edge and its streamwise gradient are shown in Fig. 3. Zero angle of attack for a given airfoil has been taken in inviscid calculation because of a long enough part of streamwise flow acceleration and, as a consequence, intense cross-flow in the boundary layer.

The boundary layer flow is determined by the velocity components u, v, w, the static pressure p, the air density ρ, the static enthalpy $h = c_p T$, and the average vibrational energy of air molecules per unit mass ω. It is assumed that the infinite set of DBD-actuators is placed on a wing surface with the step z_e in the spanwise direction, as it is shown in Fig. 4. The exposed electrodes of the actuators begin on the leading edge and are directed along the x-axis. It is

supposed that every actuator creates volumetric force and energy input distributions which do not depend on the x-coordinate. It is evident that a variation of static pressure along a wing chord will influence on discharge characteristics and, hence, on distributions of the volumetric force and energy input. But this effect is neglected in the current approximate consideration.

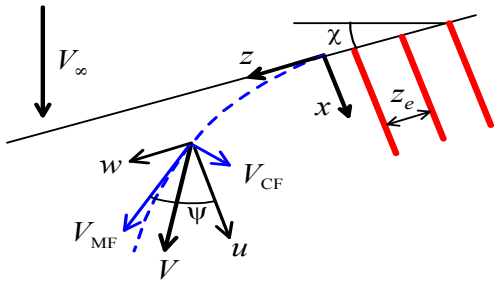

Figure 4: Decomposition of the velocity vector in boundary layer flow

In reality DBD-actuators generate both horizontal (parallel to a dielectric surface) and vertical (normal to the surface) components of the volumetric force. Theoretical estimations [16] show that the impact of the vertical force component directed to the solid surface on a boundary layer flow can be noticeable if this component is much greater than the horizontal one and is not uniform along the surface. But experiments demonstrate that the horizontal force exceeds essentially the vertical one [17]. Therefore the influence of the vertical volumetric force on a boundary layer flow is not taken onto account. A possibility to use the usual boundary layer approximation in the considered case is proved in [18]. The mentioned above characteristics of the boundary layer flow are governed by the following system of the equations and boundary conditions:

$$\frac{\partial(\rho u)}{\partial x}+\frac{\partial(\rho v)}{\partial y}+\frac{\partial(\rho w)}{\partial z}=0,\quad p=\frac{\gamma-1}{\gamma}\rho h \tag{1}$$

$$\rho u\frac{\partial u}{\partial x}+\rho v\frac{\partial u}{\partial y}+\rho w\frac{\partial u}{\partial z}=-\frac{dp}{dx}+\frac{\partial}{\partial y}\left(\mu\frac{\partial u}{\partial y}\right),\ \rho u\frac{\partial w}{\partial x}+\rho v\frac{\partial w}{\partial y}+\rho w\frac{\partial w}{\partial z}=F+\frac{\partial}{\partial y}\left(\mu\frac{\partial w}{\partial y}\right) \tag{2}$$

$$\rho u\frac{\partial h}{\partial x}+\rho v\frac{\partial h}{\partial y}+\rho w\frac{\partial h}{\partial z}=u\frac{dp}{dx}+\mu\left[\left(\frac{\partial u}{\partial y}\right)^2+\left(\frac{\partial w}{\partial y}\right)^2\right]+\frac{\partial}{\partial y}\left(\frac{\mu}{\mathrm{Pr}}\frac{\partial h}{\partial y}\right)+(1-r)Q+\rho\frac{\omega-\omega_0}{\tau_{VT}} \tag{3}$$

$$\rho u\frac{\partial \omega}{\partial x}+\rho v\frac{\partial \omega}{\partial y}+\rho w\frac{\partial \omega}{\partial z}=\frac{\partial}{\partial y}\left(\frac{\mu}{\mathrm{Sc}}\frac{\partial \omega}{\partial y}\right)+rQ-\rho\frac{\omega-\omega_0}{\tau_{VT}} \tag{4}$$

$$y=0:\ u=v=w=\partial h/\partial y=\omega=0;\quad y=y_e:\ u=u_e, w=w_e, h=h_e, \omega=0 \tag{5}$$

$$w_e=V_\infty\sin\chi,\quad h_e=h_\infty+0.5\left(V_\infty^2-u_e^2-w_e^2\right)$$

$$\mu(T) = 1.47 \cdot 10^{-6} \frac{T^{3/2}}{T+114}, \quad \gamma = 1.4, \quad \mathrm{Pr} = 0.72, \quad \mathrm{Sc} = 0.9$$

Because the boundary layer flow is assumed to be periodical along a wing span, the periodicity conditions for all flow functions are prescribed at $z = 0$ and $z = z_e$. In the system (1)-(5) F and Q are the spatial distributions of the time averaged horizontal volumetric force and total Joule dissipation generated in every actuator and determined in analytical form below, r is the fraction of Joule dissipation entering initially in vibrational degrees of freedom of nitrogen molecules and relaxing into translation degrees of freedom with the characteristic time τ_{VT}, the last terms in the equations (3) and (4) simulate the process of the vibrational-translational relaxation with the equilibrium value of the vibrational energy $\omega_0 = 0$ for relatively cold gas considered here. The wall boundary condition for enthalpy h (5) implies a thermal insulated wall.

According to numerical modeling of DBD for considered conditions [19] the fraction of the electron power channeled into vibrational exitation of nitrogen molecules averaged during one period of DBD is estimated as $r = 0.24$. The vibrational exitation of oxygen may be neglected. The value $r = 0.24$ is used in the current calculations. The time of the vibrational-translational relaxation τ_{VT} for nitrogen molecules depends on gas pressure p and temperature T according to the following expression [20]: $p\tau_{VT} = 6.5 \cdot 10^{-4} \exp(137/T^{1/3})$ Pa·s.

The analytic approximation for time averaged volumetric force and Joule dissipation is taken in the form of pyramid [21]

$$0 \le y \le y_0, \quad \frac{y}{y_0}\delta z + z_1 \le z \le z_m: \quad F = F_m\left(\frac{z-z_1}{\delta z} - \frac{y}{y_0}\right), \ \delta z = z_m - z_1 \tag{6}$$

$$0 \le y \le y_0, \quad z_m \le z \le z_2 - \frac{y}{y_0}\Delta z: \quad F = F_m\left(1 - \frac{z-z_m}{\Delta z} - \frac{y}{y_0}\right), \ \Delta z = z_2 - z_m$$

Predefined values of $\langle F_{\|} \rangle$, y_0, z_1, z_2 determine the maximal value of this distribution $F_m = 6\langle F_{\|} \rangle / [y_0(z_2 - z_1)]$. Here $\langle F_{\|} \rangle$ is the time averaged total (space integrated) horizontal force generated by every actuator per length unit of the exposed electrode measured in N/m.

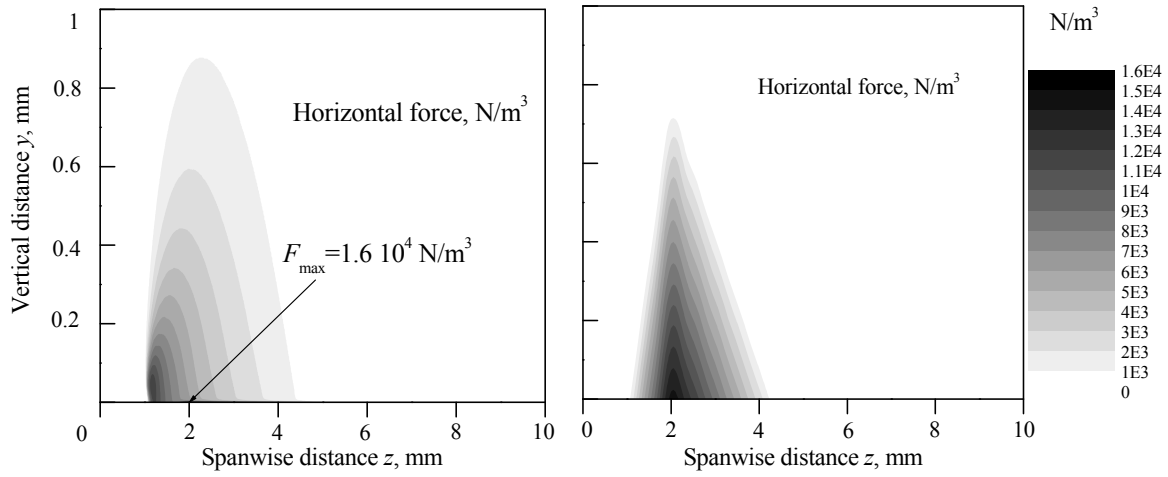

Figure 5: Comparison of calculated (left) and analytic (right) distributions of volumetric force

Figure 5 demonstrates the comparison of the volumetric force calculated on the base of DBD numerical modeling in [19] and the approximation (6) at $\langle F_{\|} \rangle = 6.74 \cdot 10^{-3}$ N/m, $y_0 = 0.8$, $z_1 = 1$, $z_m = 2$, $z_2 = 4.4$ mm.

The specified above free-stream parameters and characteristic length l determine the value of the Reynolds number $\mathrm{Re} = 2.03 \cdot 10^5$ and the boundary layer thickness on the critical line $\delta_0 \approx 5\mathrm{Re}^{-1/2} l \approx 0.33$ mm. Taking into account this small boundary layer thickness the following constant parameters determining the volumetric force and heat sources were used in calculations: the spatial period of the actuator system $z_e = 5$ mm, the vertical size $y_0 = 0.3$ mm, the horizontal sizes $z_1 = 0.5$, $z_m = 1$, $z_2 = 2.5$ mm for volumetric force distribution, and the total horizontal force generated by every actuator $\langle F_{\|} \rangle = 0.02$ N/m. According to numerical modeling of DBD-actuators [19] the spatial distribution of Joule dissipation is more sharp and narrow as compared with the force distribution. Therefore the following geometric parameters were taken for Joule dissipation source: $y_0 = 0.2$, $z_1 = 0.5$, $z_m = 0.8$, $z_2 = 1.5$ mm. The energy efficiency of DBD is defined by the relation of body force to dissipated power $E \equiv \langle F_{\|} \rangle / \langle J \rangle$ [22]. This relation depends on actuator geometry, gas pressure, other physical parameters, and is the order of 10^{-4} s/m [23]. Two values of the efficiency coefficient $E = 2.5 \cdot 10^{-4}$ and $5 \cdot 10^{-4}$ s/m are used at a given value of $\langle F_{\|} \rangle$ for evaluation of energy input $\langle J \rangle$ on boundary layer flow and its stability. The first value corresponds to E calculated in [19] and the second value seems to be rather overestimated. Nevertheless the results of numerical modeling obtained below emphasize the significance of obtaining the most high energy efficiency in any DBD system developed for considered LFC method.

Numerical solution of the system (11)-(15) at given distributions of flow parameters on the external boundary y_e has been executed with the use of the expansion of all dependent variables and volumetric sources (6) in finite Fourier series on the z-variable and subsequent solution of the resulting 2D equation systems.

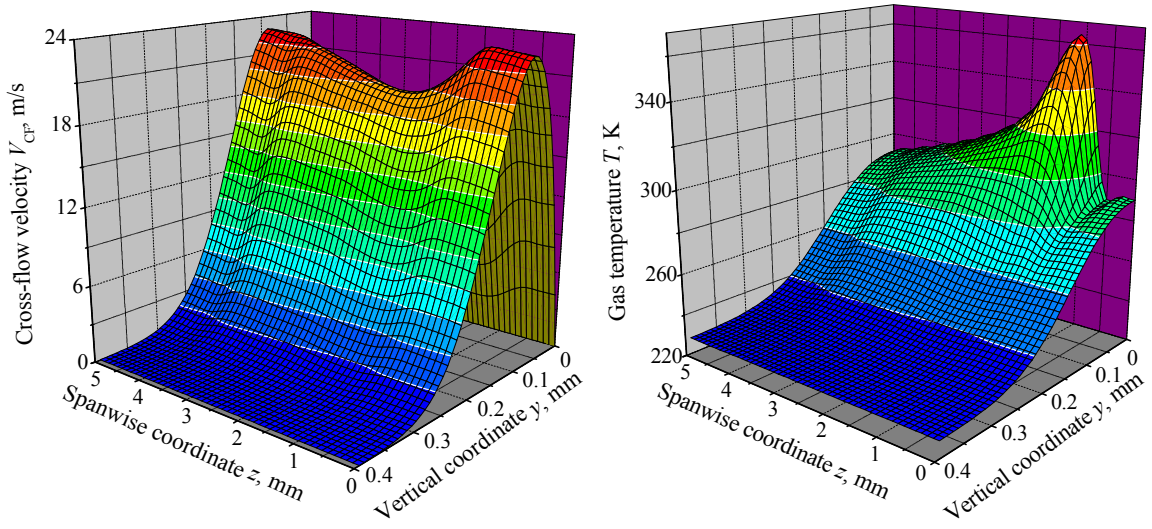

Figure 6: Distributions of the cross-flow velocity and the gas temperature in the cross-section $x/l = 1$

The boundary layer flow becomes highly non-uniform along a wing span because of force and heat impact of actuators. Figure 6 demonstrates the cross-flow velocity and the gas

temperature distributions in the streamwise cross-section $x/l = 1$ for $E = 2.5 \cdot 10^{-4}$ s/m. The cross-flow velocity V_{CF} is calculated according to

$$V_{CF} = u \sin\psi - w\cos\psi, \quad V_{MF} = u\cos\psi + w\sin\psi, \quad \mathrm{tg}\,\psi = w_e / u_e, \quad w_e = V_\infty \sin\chi \tag{7}$$

where ψ is the angle between the x-axis and the external streamline (see Fig. 4).

Two competing effects on cross-flow take place in the considered case. The volumetric force impact results in an increase in w-component and, hence, a decrease in cross-flow velocity. But a gas heating owing to Joule dissipation at a given streamwise distribution of static pressure results in a decrease in gas density and, as a consequence, an increase in u-component of gas velocity [18]. According to (7), this thermal impact leads to an increase in cross-flow velocity. The concurrence of these two effects is reflected in the left Fig. 6, showing that the maximal cross-flow velocity across a boundary layer reaches both largest and least values inside a spanwise period.

These extremal values (largest and least) are presented in Fig. 7 by dashed curves along with the average maximum of V_{CF} (calculated as zero term in appropriate Fourier series) shown by solid curves. Red curves refer to energy efficiency of actuators $E = 2.5 \cdot 10^{-4}$ s/m and blue curves refer to $E = 5 \cdot 10^{-4}$ s/m.

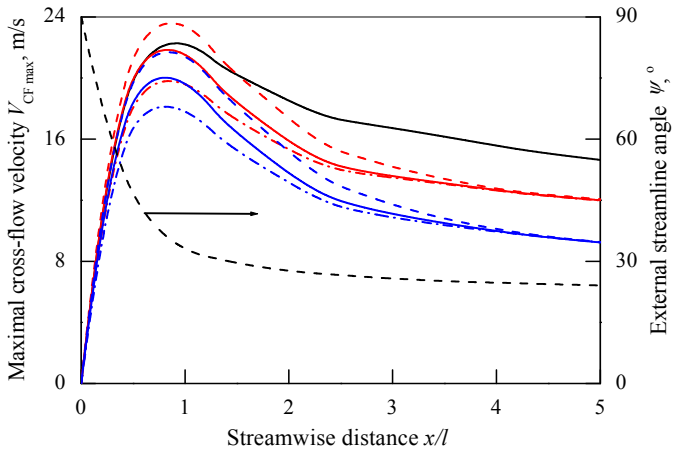

Figure 7: Maximal cross-flow velocity and the external streamline angle vs. dimensionless streamwise distance: _____ – without impact, _____ – impact at $E = 2.5 \cdot 10^{-4}$ s/m, _____ – impact at $E = 5 \cdot 10^{-4}$ s/m

First of all note that unfavorable effect of gas heating can result in the largest maximum of the cross-flow velocity exceeding the maximal V_{CF} in the boundary layer without impact of actuators in the case if their energy efficiency is not enough high. But the average maximum of V_{CF} with force and heat impact remains less than without impact in any case. The force impact resulting in an increase in w-component and a decrease in V_{CF} becomes more apparent with a decrease of the external streamline angle ψ, in accordance with (7).

At the same time the spanwise modulation of the cross-flow velocity decays downstream despite the fact that temperature nonuniformity becomes stronger, as it is seeing in Fig. 8, where the cross-flow velocity distribution in near-wall region and the gas temperature distribution across the whole boundary layer are presented for the cross-section $x/l = 3$. The characteristic feature of the cross-flow distribution in this cross-section is the presence of negative values V_{CF} near the wall. The extremal negative cross-flow velocity in near-wall

region varies from -2 m/s in the cross-section $x/l = 3$ down to -4.5 m/s at $x/l = 5$. At that the maximal temperature achieving on the wall increases up to 530 K at $x/l = 5$.

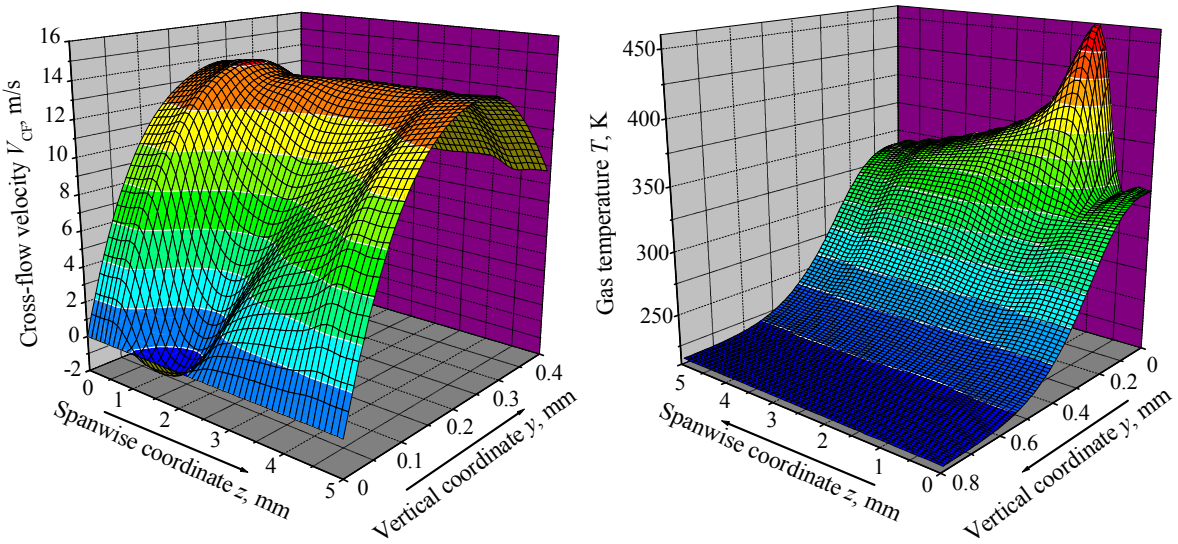

Figure 8: Distributions of the cross-flow velocity and the gas temperature in the cross-section $x/l = 3$

An increase in energy efficiency of DBD-actuators noticeably weakens negative effect of heat input on cross-flow attenuation. Three blue curves in Fig. 7 demonstrate that a force impact of actuators prevails above a heat impact in all considered part of boundary layer flow at $E = 5 \cdot 10^{-4}$ s/m. At that the extremal negative value of the cross-flow velocity in the cross-section $x/l = 5$ varies not many, namely, up to -4.8 m/s but the maximal temperature decreases remarkably down to 380 K.

3 CALCULATIONS OF CROSS-FLOW STABILITY

The influence of plasma actuators on boundary layer stability is estimated in the framework of the linear stability equation system of Dunn-Lin [24]. The spanwise spatial modulation of the boundary layer flow is not taken into account in the present simplified consideration. It means that only zero terms of Fourier expansions of undisturbed flow functions are used in the stability analysis.

Only stationary cross-flow-type disturbances are considered, which are characterized by the angle between the external streamline and the wave vector direction in the range 85-90°. The well-known e^N-method is used to estimate the position of laminar-turbulent transition [2]. So the disturbances of all flow functions and the N factor are defined as follows:

$$q(x,y,z) = q^*(y)\exp\left[i(\alpha x + \beta z)\right] = q^*(y)\exp(-\alpha_i x)\exp\left[i(\alpha_r x + \beta z)\right], \quad N(x) = -\int_{x_0}^{x} \alpha_i dx \tag{8}$$

Here q^* is the complex eigenfunction, $\alpha = \alpha_r + i\alpha_i$ is the complex eigenvalue, α_r and β represent the wavenumber components in x- and z-directions, α_i represents increment of spatial growth ($\alpha_i < 0$) or decrement of decay ($\alpha_i > 0$) of disturbances, x_0 is the initial coordinate where α_i obtains negative value, i.e. the boundary layer flow becomes unstable.

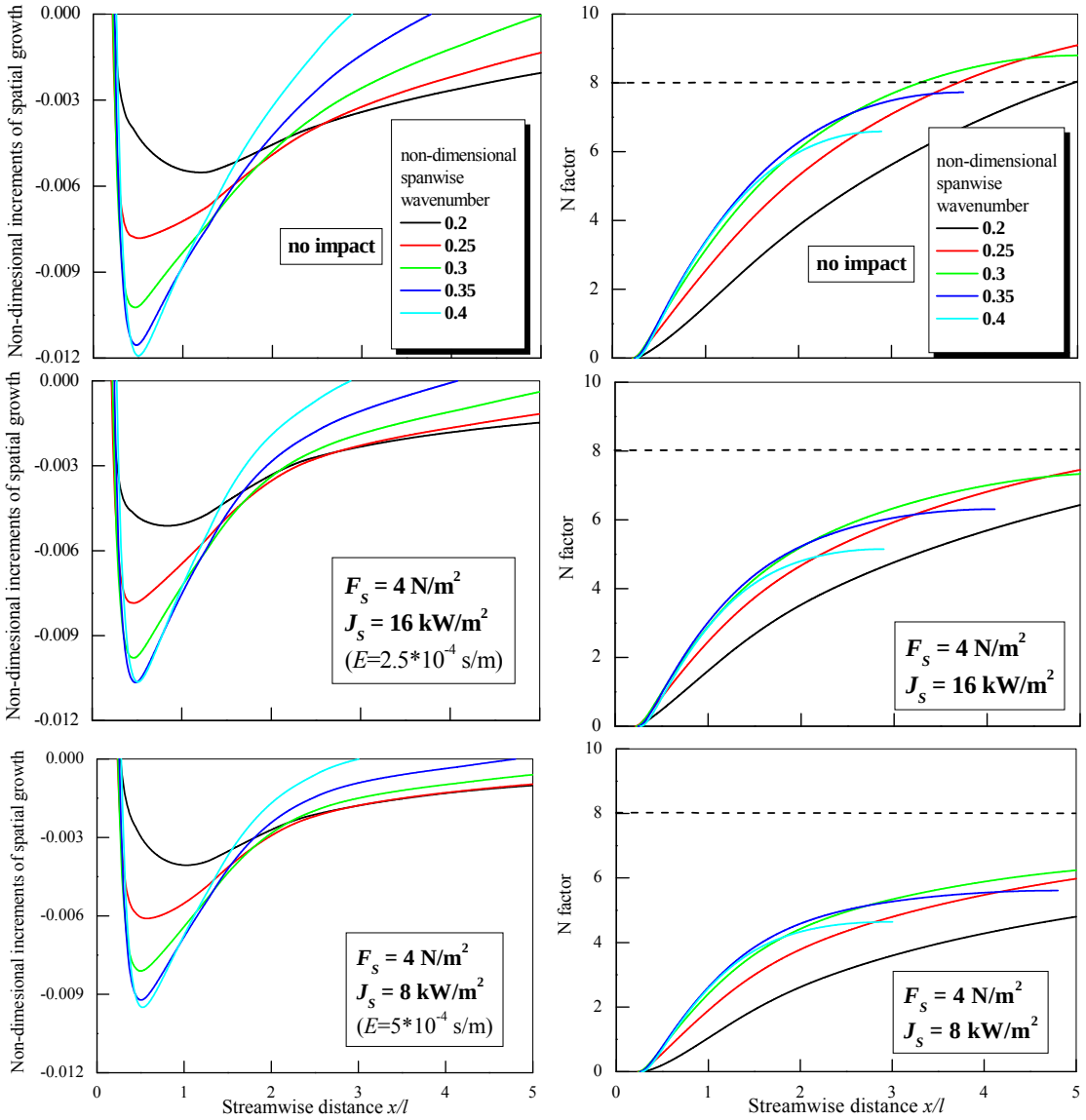

Figure 9: Streamwise distributions of non-dimensional increments of spatial growth and N factor

The so-called fixed β strategy [2] is used for N factor computation. That is the streamwise distributions of the eigenvalue α and the N factor are calculated for a set of fixed spanwise wavenumbers β. Figure 9 demonstrates calculated distributions of dimensionless increments of spatial growth $\alpha' = \alpha l \mathrm{Re}^{-1/2}$ and N factors in streamwise direction for several dimensionless spanwise wavenumbers $\beta' = \beta l \mathrm{Re}^{-1/2}$.

The e^N-method implies that laminar-turbulent transition occurs when N factor calculated according to (8) for any spanwise wavenumber reaches some predefined value N_T. The position of the cross-flow induced transition is estimated by N_T = 8-10 for the fixed β strategy used here [2]. Using the lower value N_T = 8, one can see in the right upper Fig. 9 that transition can occur in boundary layer without impact of actuators at the distance x/l = 3.3 for β' = 0.3. The legends in lower four graphs indicate the average densities of the volumetric

force and the electric power consumed per unit of a wing surface calculated according to $F_S = \langle F_{\|} \rangle / z_e$, and $J_S = \langle F_{\|} \rangle / (E\, z_e)$, respectively. Impact of actuators even at low energy efficiency $E = 2.5 \cdot 10^{-4}$ s/m prevents transition at least in the considered part of the boundary layer. An increase of energy efficiency up to $E = 5 \cdot 10^{-4}$ s/m ensures more significant reserve of flow stability. That is the volumetric force generated by actuators and, consequently, electric power needed for laminar-turbulent transition delay can be reduced appreciably if energy efficiency of DBD-actuators is high enough.

It must be noted that the average density of the electric power per unit of a wing surface in the considered case is estimated as $J_S = 16$ kW/m^2 at the energy efficiency of actuators $E = 2.5 \cdot 10^{-4}$ s/m. This power about twice as large as compared to the mechanical power required to overcome the turbulent skin friction on a wing in cruise flight. However, DBD-actuators required to remove a laminar-turbulent transition caused by cross-flow-type instability may cover only a few percent of a wing surface. Therefore, significant savings in mechanical power can be obtained due to laminarization about a half of a wing surface (approximately up to static pressure minimum) if the transition induced by Tollmien–Schlichting instability will be suppressed, for example, due to appropriate favourable streamwise pressure gradient.

4 CONCLUSIONS

- The average density of the volumetric force per unit of a wing surface of a few N/m^2 seems to be sufficient for delaying laminar-turbulent transition induced by cross-flow instability at cruise flight conditions.
- Both the boundary layer flow and the cross-flow stability characteristics are very sensitive to volumetric heat input and, hence, to energy efficiency of plasma actuators. It demands thorough optimization of DBD-actuator system including its miniaturization.

REFERENCES

[1] Abbas, A, de Vicente, J. and Valero, E. Aerodynamic technologies to improve aircraft performance. *Aerospace Sci. & Technol*. (2013) **28**:100–132.

[2] Arnal, D. and Casalis, G. Laminar-turbulent transition prediction in three-dimensional flows. *Prog. Aerospace Sci.* (2000) **36**:173–191.

[3] Chernyshev, S.L., Kiselev, A. Ph. and Kuryachii, A.P. Laminar flow control research at TsAGI: Past and present. *Prog. Aerospace Sci.* (2011) **47**:169-185.

[4] Moreau, T. Airflow control by non-thermal plasma actuators. *J. Phys. D: Appl. Phys.* (2007) **40**:605-636.

[5] Corke, T.C., Enloe, C.L. and Wilkinson, S.P. Dielectric barrier discharge plasma actuators for flow control. *Annu. Rev. Fluid Mech.* (2010) **42**:505-529.

[6] Wang, J. J., Choi, K.-S., Feng, L., Jukes, T. and Whalley, R. Recent developments in DBD plasma flow control. *Prog. Aerospace Sci.* (2013) **62**:52–78.

[7] Mack, L.M. On the stability of the boundary layer on a transonic swept wing. *AIAA Paper* 1979-264 (1979).

[8] Thomas, F.O., Corke, T.C., Iqbal, M., Kozlov, A. and Schatzman, D. Optimization of dielectric barrier discharge plasma actuators for active aerodynamic flow control. *AIAA*

Journal (2009) **47**:2169-2178.

[9] Do, H., Kim, W., Capelli, M.A. and Mungal, M.G. Cross-talk in multiple dielectric barrier discharge actuators. *Appl. Phys. Let.* (2009) **92**: 071504.

[10] Benard, N., Jolibois, J., Mizuno, A. and Moreau, E. Innovative three-electrode design for definition of multiple dielectric barrier discharge actuators. *Proceedings of 2009 Electrostatic joint Conference* (2009) Paper # P1.17.

[11] Berendt, A., Podlinski, J., and Mizeraczyk, J. Multi-DBD actuator with floating inter-electrode for aerodynamic control. *Nukleonika*. (2012) **57**:249-252.

[12] Kuryachii A.P., Rusyanov, D.A., Chernyshev, S.L. and Skvortsov, V.V. About increase of efficiency of plasma multi-actuator system for boundary layer control. *TsAGI Sci. Journal*. (2013) **44**:305-326.

[13] Chernyshev, S.L., Kuryachii, A.P., Manuilovich, S.V., Rusyanov, D.A. and Skvortsov, V.V. Attenuation of cross-flow-type instability in compressible boundary layer by means of plasma actuators. *AIAA Paper* 2013-321 (2013).

[14] Soloviev, V.R. Analytical estimation of the thrust generated by a surface dielectric barrier discharge. *J. Phys. D: Appl. Phys.* (2012) **45**: 025205.

[15] Fedorov, A.V., Krivtsov, V.M., Soloviev, V.R. and Soudakov, V.G. Modeling of aerodynamic forcing induced by surface dielectric barrier discharge. *AIAA Paper* 2011-158 (2011).

[16] Kuryachii, A. P. Effect of a space-time source structure simulating a dielectric barrier discharge on the laminar boundary layer. *Fluid Dynamics*. (2006) **41**:366-374.

[17] Benard, N., Debien, A. and Moreau, E. Time-dependent volume force produced by a non-thermal plasma actuator from experimental velocity field. *J. Phys. D: Appl. Phys.* (2013) **46**: 245201.

[18] Kuryachii, A.P., and Manuilovich, S.V. Attenuation of cross-flow-type instability in a 3D boundary layer due to volumetric force impact. *TsAGI Sci. Journal*. (2011) **42**:345-360.

[19] Chernyshev, S.L., Kuryachii, A.P., Manuilovich, S.V., Rusyanov, D.A. and Skvortsov, V.V. On a possibility of laminar flow control on a swept wing by means of plasma actuators. *CD-ROM Proceedings of the 5th European Conference for Aeronautics and Space Sciences* (*EUCAS 2013*) ISBN: 978-84-941531-0-5.

[20] Mnatsatanyan, A.H., and Naigis, G.V. Balance of the vibrational energy in discharges in air. *High Temperature*. (1985) **23**:640-648.

[21] Kuryachii, A.P. Control of cross flow in the three-dimensional boundary layer using space-periodic body force. *Fluid Dynamics.* (2009) **44**:233–239.

[22] Porter, C., Baughn, J., McLaughlin, T., Enloe, C., and Font, G. Temporal force measurements on an aerodynamic plasma actuator. *AIAA Paper* 2006-104 (2006).

[23] Kuryachii, A.P., Rusyanov, D.A. and Skvortsov, V.V. Modeling of dielectric barrier discharge actuators at various gas pressures and estimation of their influence on shear flows. *TsAGI Sci. Journal*. (2011) **42**:227-243.

[24] Dunn, D.W., and Lin, C.C. The stability of the laminar boundary layer in a compressible fluid for the case of three-dimensional disturbances. *J. Aeronautical Sci.* (1952) **19**:491–502.